Circulation: Heart Failure

ORIGINAL ARTICLE

Modeling Heart Failure With Preserved Ejection Fraction Using Human Induced Pluripotent Stem Cell–Derived Cardiac Organoids

Idan Refael Haim, MSc; Amit Gruber, MD, PhD; Noam Kazma, MSc; Caroline Bashai, Msc; Hava Lichtig Kinsbruner, PhD; Oren Caspi, MD, PhD

BACKGROUND: The therapeutic armamentarium for heart failure with preserved ejection fraction (HFpEF) remains notably constrained. A factor contributing to this problem could be the scarcity of in vitro models for HFpEF, which hinders progress in developing new therapeutic strategies. Here, we aimed at developing a novel, comorbidity-inspired, human, in vitro model for HFpEF.

METHODS: Human induced pluripotent stem cells–derived cardiomyocytes were used to produce cardiac organoids. The generated organoids were then subjected to HFpEF-associated, comorbidity-inspired conditions, such as hypertension, diabetes, and obesity-related inflammation. To assess the development of HFpEF pathophysiological features, organoids were thoroughly evaluated for their structural, functional, electrophysiological, and metabolic properties.

RESULTS: Exposure to the combination of all comorbidity-mimicking conditions resulted in the largest cellular volume of 1692±52 versus 1346±84 μm^3 in RPMI (Roswell Park Memorial Institute medium) control group (P=0.003), while lower in obesity, hypertension, and diabetes groups: 1059±40 μm^3 (P=0.014), 1276±35 μm^3 (P=0.940), and 1575±70 μm^3 (P=0.146), respectively. Similarly, ultrastructural fibrosis was most significantly observed after exposure to the combination of all HFpEF-inducing conditions 14.6±1.2% compared with single condition exposure 5.2±1.3% (obesity), 6.7±3.5% (hypertension), and 9.0±1.1% (diabetes; P<0.001). Moreover, HFpEF-related conditions led to an increase in passive force compared with control (7.52±1.08 versus 2.33±0.46 mN/mm, P<0.001), whereas no significant alterations were noted in active contractile forces. Relaxation constant τ was significantly prolonged after exposure to HFpEF conditions showing a prolongation of 95.9 ms (36.4–106.4; P=0.028) compared with a shortening of 35.6 ms (43.3–67.3; P=0.80) in the control. Finally, organoid exposure to HFpEF conditions led to a significant increase in oxidative stress levels and a significant decline in oxygen consumption rate.

CONCLUSIONS: We established a novel, human, in vitro model for HFpEF, based on comorbidity-inspired conditions. The model faithfully recapitulated the structural, functional, and mechanistic features of HFpEF. This model holds the potential to provide mechanistic insights and facilitate the identification of novel therapeutic targets.

Key Words: heart failure ■ hypertension ■ induced pluripotent stem cells ■ obesity ■ organoids

Heart failure is a growing pandemic affecting over 2% of the population leading to high rates of morbidity and mortality.[1] Heart failure with preserved ejection fraction (HFpEF) is a multifactorial disease associated with significant morbidity and mortality along with detrimental impacts on quality of life.[2] HFpEF constitutes half of all heart failure cases, but unlike heart failure with reduced ejection fraction, there are almost no treatments for HFpEF that improve survival.[3] One contributing factor to this issue may arise from the limited availability of in vitro models for HFpEF, which hampers the advancement of new therapeutic approaches. Although some in vivo models have been

Correspondence to: Oren Caspi, MD, PhD, Heart Failure Unit, Department of Cardiology, Rambam Health Care Campus and B. Rappaport Faculty of Medicine, Technion, PO Box 9602, Haifa 31096, Israel. Email o_caspi@rmc.gov.il

Supplemental Material is available at https://www.ahajournals.org/doi/suppl/10.1161/CIRCHEARTFAILURE.124.011690.
For Sources of Funding and Disclosures, see page 308.

Circulation: Heart Failure is available at www.ahajournals.org/journal/circheartfailure

WHAT IS NEW?

- Existing models for deciphering the pathogenesis of heart failure with preserved ejection fraction (HFpEF) and identifying potential novel therapeutic targets remain limited.
- This study presents an in vitro model of HFpEF, generated with human cardiac organoids to emulate the disease.
- The development of the model was inspired by mimicking in vitro the comorbidities commonly associated with HFpEF, this multihit model effectively reproduces essential HFpEF features, including diastolic dysfunction with preserved contractile forces, increased passive tension, mitochondrial dysfunction, and oxidative stress.

WHAT ARE THE CLINICAL IMPLICATIONS?

- HFpEF is characterized by high morbidity and mortality, with few survival-improving therapies available—unlike heart failure with reduced ejection fraction.
- The absence of a suitable human-based HFpEF model has likely posed a barrier to drug discovery efforts.
- Developing an in vitro HFpEF model using human cardiac organoids holds great potential for uncovering the key mechanisms involved in the disease and identifying new therapeutic targets.
- This model can support both broad-based and patient-specific drug screening approaches.

Nonstandard Abbreviations and Acronyms

Ct	cycle threshold
cTnT^{+ve}	cardiac troponin T positive
DAPI	4′,6-diamidino-2-phenylindole
hCOs	Human cardiac organoids
HFpEF	Heart failure with preserved ejection fraction
hIPSC	human induced pluripotent stem cells
iNOS	Inducible nitric oxide synthase
NOS2	Nitric oxide synthase 2
NT-proBNP	N-terminal pro-B-type natriuretic peptide
OCR	Oxygen consumption rate
PCR	Polymerase chain reaction
ROS	reactive oxygen species
SERCA	Sarcoplasmic/endoplasmic reticulum Ca^{+2} ATPase
XBP1s	spliced Xbox-binding protein 1
XBP1u	unspliced Xbox-binding protein 1
ZSF1	Zucker fatty spontaneously hypertensive F1 hybrid rat

recently suggested,[4–7] there are currently no models based on human tissues which could further impede the identification of relevant novel therapeutic targets. An additional complexity in the modeling of HFpEF arises from the multifactorial nature of the disease, commencing from the confluence of various comorbidities, including but not limited to obesity, hypertension, and diabetes.[1,8]

In terms of functionality, HFpEF is characterized by diastolic dysfunction,[3] including prolonged relaxation, and increased stiffness accompanied by calcium mishandling.[9,10] This presentation is associated with various intracellular mechanisms, including oxidative stress[11,12] leading to endoplasmic reticulum stress[13] and compromised energetics.[14] Reactive oxygen species (ROS) are known to be elevated and associated with mitochondrial dysfunction, resulting in diminished ATP content.[15] These mechanisms trigger several downstream pathological conditions, such as hypertrophy and ultrastructural fibrosis, ultimately culminating in the well-recognized diastolic dysfunction characteristic of HFpEF.

The recent development of technologies based on organoids from human induced pluripotent stem cells (hIPSCs) resulted in a paradigm shift in the drug discovery arena and resulted in the identification of multiple potential therapies for genetic cardiomyopathies.[16–18] Although this technology has played a crucial role in addressing genetic cardiomyopathies, studies showcasing its applicability to acquired and multifactorial diseases are scarce.[19] In this study, we aimed at inducing HFpEF in vitro by subjecting human cardiac organoids (hCOs) to conditions inspired upon the known comorbidities leading to HFpEF.

METHODS

Data Availability Statement

The authors declare that all supporting data are available within the article and its Supplemental Material.

hIPSCs Derivation

All relevant studies were approved by the Helsinki committee of RAMBAM Medical Center, Haifa, Israel. Two distinct lines of patient-specific induced pluripotent stem cells (hIPSCs) were generated from biopsies obtained from 2 healthy volunteers, a male and a female. Reprogramming of skin fibroblasts was achieved through retrovirus delivery of the reprogramming factors KLF4 (Krüppel-like factor 4), SOX2 (SRY-box transcription factor 2), and OCT4 (octamer-binding transcription factor 4),[20,21] as previously described by our group.[22,23] All cell lines used in this study were shown to have normal karyotype.

hIPSC Culture

The hIPSCs were cultured as monolayers on 6-well plates, precoated with growth factor–reduced Cultrex (R&D Systems), and maintained in mTESR Plus medium (Thermo Fisher Scientific) in a humidified incubator (5% CO_2, 37 °C). Passaging was performed every 3 to 4 days, with dissociation using a 0.5 mM

EDTA solution (Life Technologies) at a 1:10 to 1:14 ratio. Cell cultures were tested routinely for mycoplasma using MycoBlue Mycoplasma Detector (Nanjing Vazyme Biotech, Co, China).

hIPSCs-Derived Cardiomyocytes Differentiation

The differentiation process commenced on day 0 when hIPSCs, reaching an 80% cell confluence, were subjected to 6 μM CHIR99021 (R&D Systems) in CDM3 (chemically defined medium 3) medium for a duration of 48 hours. On day 2, the medium was replaced, and 2 μM of WNT (Wingless and Int-1)-C59 (Selleck Chemicals) was applied. Subsequently, on day 4, the medium was shifted to RPMI 1640 (Roswell Park Memorial Institute medium; Thermo Fisher Scientific) supplemented with B-27 minus insulin (Thermo Fisher Scientific) and 1% penicillin/streptomycin (Biological Industries Beit-Haemek, Israel). The cultivation conditions persisted with RPMI supplemented with B-27 and 1% penicillin/streptomycin being refreshed on day 7. From day 9 onward, the differentiation milieu returned to CDM3, with a regular refreshing interval of every 2 days.

CDM3 Medium

CDM3 medium was prepared with RPMI 1640, 500 μg/mL recombinant human albumin (Thermo Fisher Scientific), 213 μg/mL L-ascorbic acid 2-phosphate, and 1% penicillin/streptomycin (Biological Industries Beit-Haemek, Israel).

Micro-Organoids Construction

hIPSCs-derived cardiomyocytes were detached using TrypLE express X1 (Thermo Fischer Scientific) for 5 minutes at 37 °C. The detached cells were seeded on a V-bottom 96-well plate (Thermo Fisher Scientific) in a concentration of 10^4 cells/50 μL for each well. Microplates were then centrifuged for 10 minutes at 200*g*. Micro-organoids were incubated at 37 °C, 5% CO_2 for 3 days with RPMI–B-27 media without insulin. The medium was refreshed every 48 hours.[24]

Cardiac Organoids Media

The media was based on DMEM medium without glucose (Thermo Fischer) with 3 mM glucose (Merk) added and supplemented with B-27 minus insulin (Thermo Fisher Scientific), 0.5% free fatty acids in the form of Albumax (Thermo Fischer Scientific) 10 mM lactate (Merk), 5 μg/mL B12-vitamin, 0.82 μM biotin, 5 mM creatine monohydrate, 2 mM taurine, 2 mM L-carnitine, 0.5 mM ascorbic acid (all from Merk), 1% KOSR (knock-out serum replacement), and 1% nonessential amino acids, 100 ng/mL dexamethasone, 4 nM Triiodo–L-thyronine (all from Thermo Fischer Scientific), and 1% penicillin/streptomycin (Biological Industries Beit-Haemek, Israel).

HFpEF Induction

Cardiomyocytes in 2-dimensional cultures, micro-organoids, and the passively stretched human cardiac organoids (hCOs) were all cultured in basal cardiac organoids medium with added factors emulating the comorbidities associated with HFpEF: obesity-related inflammation, diabetes, and hypertension and were referred to as HFpEF-inducing conditions. To emulate obesity-related inflammation, inflammatory cytokines 10 ng/mL IL (interleukin)-1β and 100 ng/mL IFN (interferon)-γ (Thermo Fisher Scientific) were added to the medium. Diabetic conditions were modeled by using high glucose concentration (11.1 mmol/L) with insulin deprivation. Finally, hypertension was emulated by using 10 ng/mL angiotensin-II and 10 ng/mL endothelin-1 (both from Merck). All cells and organoids were exposed to the HFpEF-inducing conditions for 7 days.

Micro-Organoids Optical Characterization

Organoids were assessed using an automated imaging system. ORCA-Flash 4.0 camera (Hamamatsu, Japan) was mounted on an Olympus IX83 microscope with ×4/0.16 objective (Olympus, Japan). Organoids were automatically scanned using the TANGO Desktop stage controller (Märzhäuser Wetzlar, Germany). Cross-sectional area of the organoids was analyzed using Cell Profiler software (Broad Institute).[25]

Fibrosis Analysis

Micro-organoids were grown in HFpEF-inducing conditions and isolated comorbidity–mimicking conditions. The organoids were then fixed using 4% paraformaldehyde. Micro-organoids were sectioned by a blinded technician followed by Masson trichrome staining. For the evaluation of fibrosis, the center of each organoid was selected to represent the largest area. Imaging was conducted using a panoramic 250 Flash III automatic slide scanner (3DHISTECH, Hungary). Fibrosis was evaluated using an automated process based on a sequence of modules performed in Cell Profiler software (Broad Institute)[25] as outlined in Figure S1.

hCOs Construction

A mixture of 2 million cells in hCOs construction media, with bovine collagen (LLC Collagen solutions, Britain), 2× DMEM, and 0.1 NaOH for pH neutralization was cast in a ring-shaped mold. After 3 days of condensation, the construct was transferred to a passive stretching device, with cardiac organoids media medium refreshed every 2 days, as previously described.[26] The hCOs were used in experiments only after 1 week in the passive stretching device, to allow for tissue compaction. The 2× DMEM media was composed of 40% 5× DMEM, 40% FBS (both from Biological Industries Beit-Haemek, Israel), 15% H_2O, 1% glutamine, and 1% penicillin/streptomycin.

hCOs Construction Media

The medium was based on Iscove-Medium (Biological Industries Beit-Haemek, Israel) with 20% FBS, 1% nonessential amino acids (Thermo Fisher Scientific), 1% L-glutamine (Thermo Fisher Scientific), 1% penicillin/streptomycin, and 0.1 μmol/mL β-mercaptoethanol (Thermo Fisher Scientific).

hCOs Force-Length Evaluation

Force of hCOs was measured using a force transducer with a length controller by Aurora Scientific (Canada), in Tyrode's solution (140 mmol/L NaCl, 5.4 mmol/L KCl, 1 mmol/L $MgCl_2$, 10 mmol/L glucose, 1.8 mmol/L $CaCl_2$, 10 mmol/L HEPES, pH 7.4 with NaOH at 25 °C). Tissues were paced at 1 Hz and were stretched over 2 hooks every 10 seconds by 0.1 mm up to a 0.8 mm maximal stretch, followed by return to basal 0 mm stretch. To ensure accurate measurement of passive force, the final 3 seconds after each stretch were recorded as the stretch-induced

passive force, mitigating potential transient changes that may occur immediately after tissue stretching. To exclude differential tissue relaxation dynamics after each stretching step (the inherent viscoelastic relaxation of the tissue) between the studied groups we calculated the exponential decay constant of the passive force, tau (τ), after each lengthening step. For this purpose, we applied a low pass filter (gaussian, low pass filter 0.2 Hz) analyzing solely the alteration of the passive force without the active contractions (Clampfit 10.7 software) and calculated the tau (τ) of the decay in passive force.

Immunofluorescence Staining

Cardiomyocytes and organoids exposed to HFpEF-inducing conditions and control organoids media were stained for DAPI (4′,6-diamidino-2-phenylindole; dilution of 1:1000, CAS: 28718-90-3, from Merk) and cTnT (cardiac troponin T; dilution of 1:250, CAS: AB91605, Abcam, Britain).

3-Dimensional Micro-Organoid Size Analysis

Micro-organoids were stained as full tissues and scanned in z-stack using an LSM900 confocal microscopy platform (Zeiss, Germany).[27] The scans were analyzed via Imaris software for their total volume and their nuclei quantity. Each micro-organoid volume was normalized to the nuclei quantity to detect hypertrophy rather than hyperplasia.

hCO Cellular Hypertrophy Evaluation

To assess for cellular hypertrophy within the hCOs after exposure to HFpEF, we quantified the relative $cTnT^{+ve}$ (cTNT positive) area per nuclei (stained using DAPI) within the area in representative sections of the hCOs.

Calcium Imaging

Cardiomyocytes were dissociated and seeded on a 35-mm Glass bottom dish with 10 mm microwell #1.5 cover glass (Cellvis) as single cells (50 000 cells/mL). Calcium imaging was performed using Fluo-4 calcium dye (Thermo Fisher Scientific) in an LSM900 confocal microscopy platform (Zeiss, Germany).[27]

N-Terminal Pro-B-Type Natriuretic Peptide Measurement

NT-proBNP (N-terminal pro-B-type natriuretic peptide) was measured using an NT-proBNP kit and Abbott ARCHITECT analyzer (Abbot Laboratories) from the 1:20 diluted media of the passively stretched organoids.

ATP Content

Cells were seeded on a 96 optic plate (Thermo Fisher Scientific) and analyzed for their ATP content using CellTiter-Glo 2.0 Assay kit (Promega) following the manufacturer's instructions. The ATP content was assessed via Infinite M200 PRO plate reader (Tecan Trading AG, Switzerland).

Sea Horse Metabolic Assay Test

Cardiomyocytes were seeded at 50 000 cells/well density in Seahorse XF cell culture plates (By Agilent), ensuring even distribution across the wells. The cells were exposed to HFpEF-inducing conditions and cardiac organoid media as a control. The instrument automatically records the oxygen consumption rate (OCR) as an indicator of mitochondrial respiration. The OCR was analyzed using Wave 2.6.3 (By Agilent).[28]

ROS Measurement

Cardiomyocytes were seeded and allowed to attach in a 96-well plate and analyzed for their ROS content via DCFDA/H2DCFDA (2',7'-dichlorodihydrofluorescein diacetate)–Cellular ROS Assay Kit (Abcam, Britain). The quantification of fluorescence intensity indicative of ROS levels was performed using Infinite M200 PRO plate reader (Tecan Trading AG, Switzerland).

Quantitative Real-Time Polymerase Chain Reaction

For quantitative real-time polymerase chain reaction (PCR), total RNA was purified with Bio-Tri Reagent (BioLabs, Israel) following the manufacturer's extraction protocol. RNA (1 µg) underwent reverse transcription using Iscript cDNA Synthesis Kit (Bio-Rad). Quantitative real-time PCR was performed using LightCycler 480 SYBR Green I Master (Roche, Switzerland). StepOnePlus Real-Time PCR System (Thermo Fisher Scientific) was used to assess gene expression levels. Results were analyzed using the comparative cycle threshold (Ct) method. Analysis employed the comparative Ct method, generating ΔCt values by subtracting the Ct of the housekeeping gene *GAPDH* Ct from each mRNA Ct in every sample. Relative expression was calculated using 2^(ΔΔCt). The primer list is available in the Table S1.

Statistical Analysis

Shapiro-Wilk test was used to assess whether the data are distributed normally. Normally distributed data sets are presented as mean±SEM. Non-normally distributed data are presented as median and interquartile range (IQR). Comparisons among groups were analyzed with 2-tailed Student *t* test or ANOVA for normally distributed data and Mann-Whitney *U* test and Kruskal-Wallis for non-normally distributed data. For repeated measurements, 2-way repeated measure ANOVA was performed, followed by least square means with Dunn-Sidak correction in post hoc. Whenever multiple comparisons were performed, the post hoc Tukey test was used. For the evaluation of force-length relationships in hCOs, the Pearson correlation coefficient was calculated, and a linear regression model was used. Data are displayed as XY scatter plots or box plots. $P<0.05$ was considered significant. The statistical analysis was performed using GraphPad Prism 9.5.1.

RESULTS

To evaluate the contribution of the conditions mimicking HFpEF-related comorbidities on HFpEF induction, micro-organoids (10^4 cells per organoid) were initially utilized. The micro-organoids were exposed to comorbidity-inspired inducing conditions commonly associated with HFpEF: hypertension, obesity-related inflammation, and diabetes. The effect of each isolated condition

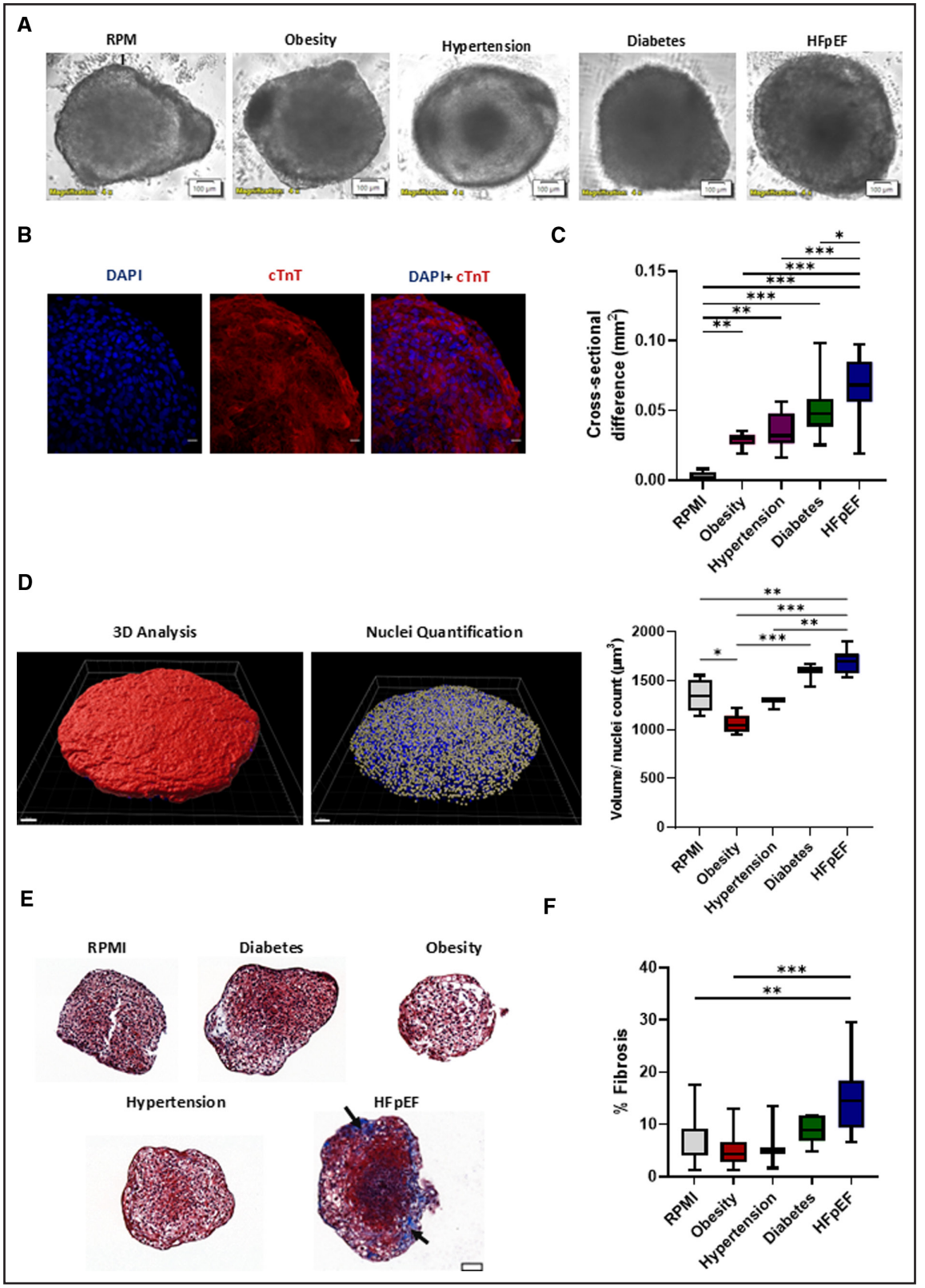

Figure 1. Ultrastructural analysis of micro-organoids.

A, Bright-field images of the micro-organoids, during relaxation. Scale bar: 100 µm. **B**, Immunofluorescent staining of a micro-organoid, cTnT (cardiac troponin T) in red, DAPI (4′,6-diamidino-2-phenylindole) in blue. Scale bar: 20 µm. **C**, Cross-sectional area differences as calculated from bright-field images, taken before and after treatment, in mm². The biological replicate numbers in RPMI (Roswell Park Memorial Institute medium), obesity, hypertension, diabetes, and heart failure with preserved ejection fraction (HFpEF) groups were 9, 12, 6, 13, and 26, respectively. Measured as the difference between micro-organoids postexposure and their preexposure size. **D**, Micro-organoids (*Continued*)

was evaluated and compared with the control medium, RPMI–B-27, and to the combination of all conditions associated with HFpEF. Organoid morphology on bright-field imaging is depicted in Figure 1A.

Initially, the micro-organoids exposed to HFpEF-mimicking conditions were evaluated for the presence of hypertrophy and ultrastructural fibrosis, among the key hallmarks of HFpEF. Micro-organoids were stained for cTnT and DAPI to assess the cardiomyocyte cell density and viability (Figure 1B). After 1 week of exposure to obesity-, hypertension-, and diabetes-mimicking conditions, the cross-sectional area of the organoids during maximal relaxation was increased by 0.03±0.001 mm^2 (P=0.003), 0.04±0.006 mm^2 (P=0.002), and 0.05±0.005 mm^2 (P<0.001), respectively, when compared with 0.003±0.001 mm^2 increase in control RPMI. Notably, the combined exposure to all HFpEF conditions resulted in the most substantial size augmentation: 0.07±0.004 mm^2 (P<0.001) compared with obesity (P<0.001), hypertension (P<0.001), diabetes (P=0.030), and RPMI (P<0.001; Figure 1C; Table S2). To assess for cellular hypertrophy, we initially evaluated the effect of exposure of single-cell cardiomyocytes to HFpEF-inducing conditions. Immunofluorescence staining of cardiomyocytes as single cells (Figure S2A) revealed significant hypertrophy of cardiomyocytes exposed to the HFpEF conditions: 5934 μm^2 (IQR, 2240–9757) versus 2391 μm^2 (IQR, 1544–3542) for control (P=0.023; Figure S2B; Table S3). To further analyze tissue hypertrophy, the micro-organoids were stained as full tissues and evaluated for their 3-dimensional volume, normalized to nuclei content (Figure 1D). HFpEF organoids demonstrated the largest volume of 1692±52 μm^3 versus 1346±84 μm^3 in the RPMI control group (P=0.003; Figure 1D; Table S4). The diabetes group demonstrated a slightly larger, but not statistically significant, volume of 1575±70 μm^3 (P=0.146), as well as the hypertension group with an average volume of 1276±35 μm^3 (P=0.940). The obesity group demonstrated a significantly smaller volume of 1059±40 μm^3 (P=0.014). Three-dimensional volumes of the micro-organoids without nuclei number normalization after the various HFpEF-inducing conditions demonstrated a similar trend with insignificant changes, but a similar trend in terms of nuclei quantity (Figure S3A and S3B; Table S5). The organoid fibrosis burden was quantified using automated image processing analysis for a Masson trichrome staining (Figure 1E). Among the evaluated conditions, a significant increase in fibrosis burden was observed solemnly after exposure to the combined HFpEF comorbidities, when compared with control group RPMI: 14.6±1.2% fibrosis burden for the HFpEF organoids versus 6.8±1.5% in RPMI, P=0.001. Fibrosis burden for obesity, hypertension, and diabetes were 5.2±1.3% (P=0.96), 6.7±3.5% (P>0.99), and 9.0±1.1% (P=0.91), respectively, compared with RPMI group (Figure 1F; Table S6).

To further investigate the impact of HFpEF-inducing conditions on intricate cardiac physiological properties, length-force dynamics were assessed using a large-scale, ring-shaped organoid model (2×10^6 cells per organoid; Figure 2A). The hCOs platform facilitates the evaluation of the organoid's passive stiffness through preload stretching (Figure S4A). In addition, for each preload length, both passive and active forces were directly measured using a force transducer (Figure 2A). Assessment of passive forces across escalating preload tissue lengths demonstrated a linear correlation between the 2 with Pearson R correlation of 0.666 and 0.583 for HFpEF and control organoids, respectively. Importantly, the slope of the HFpEF regression model was significantly higher, compared with control, indicating elevated tissue stiffness: 7.52±1.08 versus 2.33±0.46 mN/mm (P<0.001; Figure 2C and 2B; Table S7). The maximal passive force, at a tissue stretch of 0.8 mm was significantly higher in HFpEF organoids: 3.93 mN (IQR, 3.56–10.00) versus 1.20 mN (IQR, 0.95–3.33), respectively, (P=0.03; Figure 2D; Table S8). To evaluate whether differences in the inherent viscoelastic relaxation properties (after each stretching step) influenced passive force measurements at steady state, the dynamics of the poststretch viscoelastic relaxation were evaluated. Although significant differences were detected in the developed passive force at steady state between HFpEF and Control hCOs, no significant changes were detected in the viscoelastic relaxation dynamics of the tissues poststretching steps. The tau constant for viscoelastic relaxation was 1969±127 ms in HFpEF-hCOs and 2136±144 ms in the control hCOs (P=0.429; Figure S4A and S4B). Although passive force was higher in the HFpEF-hCOs, we did not identify significant changes in active force between the HFpEF-hCOs and control hCOs. Linear regression of active contractile force through a series of preload stretches revealed the preservation of active force. With minimal preload (denoted as a stretch of 0 mm), the hCOs demonstrated 0.58±0.10 mN in HFpEF-hCOs versus 0.65±0.17 mN in control (P=0.13; Figure 2E; Table S9). In addition, the change of active force as a function of length was evaluated. There was no significant change in the slope of active force as function of length of the hCOs (escalating

Figure 1 Continued. 3-dimensional (3D) hypertrophy evaluation. **Left**, Representative 3D volume and nuclei quantification of volume of micro-organoids, presenting cTnT in red and DAPI in blue. Scale bar: 50 µm. **Right**, Statistical analysis of micro-organoids' volume divided by nuclei quantity, in μm^3. The biological replicate numbers in RPMI, obesity, hypertension, diabetes, and HFpEF groups were 4, 6, 3, 3, and 6, respectively. **E**, Masson trichrome staining of micro-organoids. Arrows point at collagen deposits. Scale bar: 50 µm. **F**, Statistical analysis of fibrosis percentage out of total micro-organoids size. The biological replicate numbers in RPMI, obesity, hypertension, diabetes, and HFpEF groups were 11, 8, 3, 6, and 24, respectively. One-way ANOVA was performed for the experiments in **C**, **D**, and **F**. *P<0.05, **P<0.01, ***P<0.001.

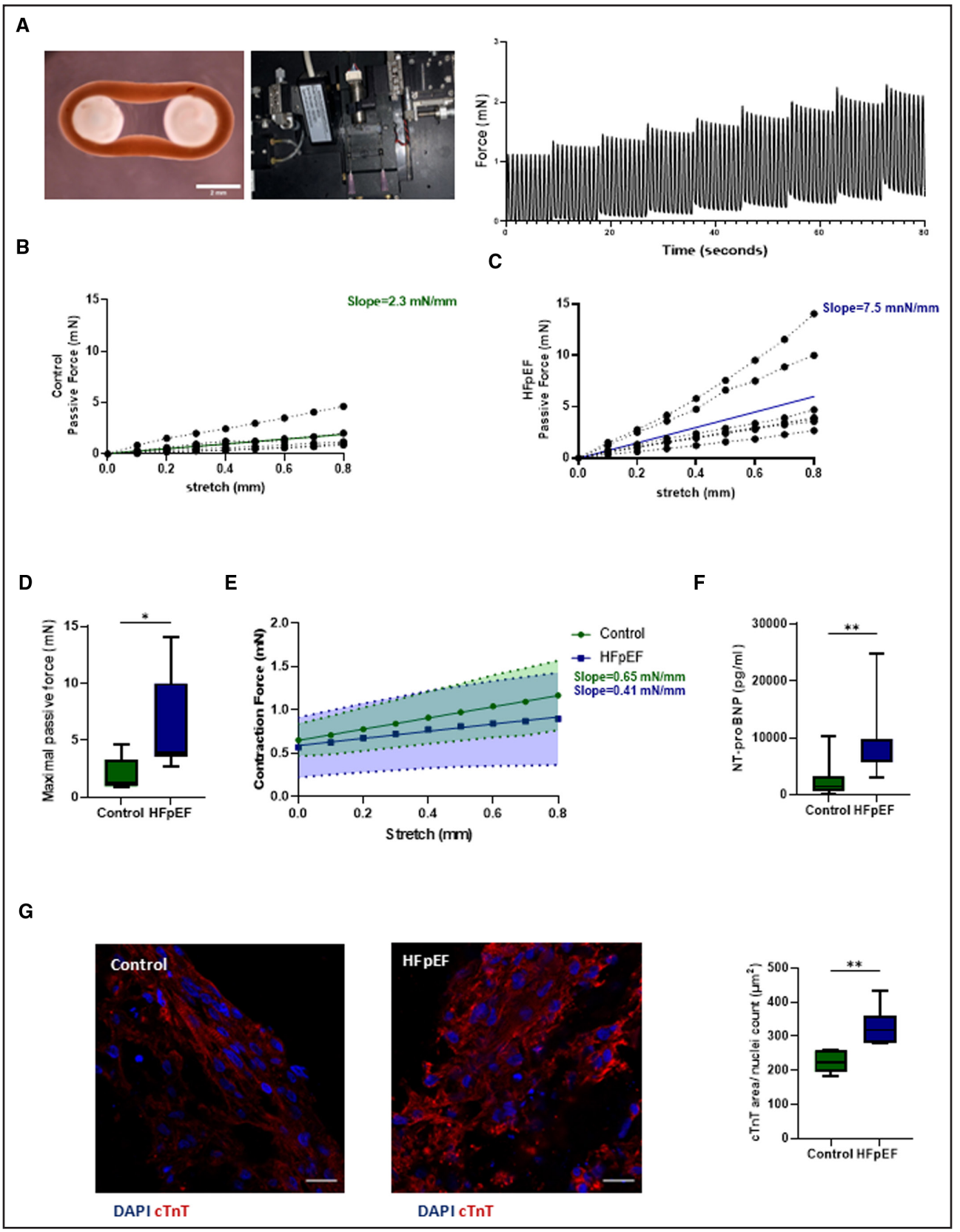

Figure 2. Assessment of heart failure with preserved ejection fraction (HFpEF)–associated characteristics in human cardiac organoids (hCOs).

A, The settings of the experiment. **Left**, A representative image of the ring-shaped hCOs. **Middle**, The force transducer coupled with the length controller used in the experiment. **Right**, A representative force-length experiment, paced at 1 Hz and stretched in a series (*Continued*)

preloads according to the Frank-Starling effect) between HFpEF-hCOs and control hCOs: 0.41±0.21 mN/mm stretch versus 0.65±0.36 mN/mm stretch (P=0.55; Figure 2E; Table S9), respectively. Furthermore, the mean NT-proBNP levels were significantly increased in hCOs after exposure to HFpEF conditions and were measured as 5956 (IQR, 5682–9848) pg/mL compared with 1440 (IQR, 686–3153) pg/mL in the control group (P=0.008; Figure 2F; Table S10). To assess for cellular hypertrophy within the hCOs, we quantified the cell size of cardiomyocytes by assessing the average sarcomeric area per nuclei using cTnT^{+ve} immunostaining and DAPI. The average sarcomeric area was significantly higher after exposure to HFpEF-inducing conditions, reflecting hypertrophy: 363.5±17.2 μm^2 versus 281.2±25.3 μm^2 in the control (P=0.022; Figure 2G; Table S11).

Diastolic relaxation properties were evaluated by measuring τ (tau), the relaxation time constant. With HFpEF conditions, τ was significantly prolonged compared with preexposure baseline from 76.7 ms (IQR, 71.0–90.0 ms) to 166.8 ms (IQR, 123.0–1837 ms; P=0.028) versus a shortening from 122.6 ms (IQR, 108.0–130 ms) to 97.1 ms (IQR, 53.3–154.1 ms) in the control group (P=0.80; Figure 3A; Table S12). To elucidate whether the prolongation of relaxation is associated with calcium handling abnormality, Ca^{+2} transients in single cells were analyzed optically using confocal microscopy (Figure 3B). Exposure to HFpEF conditions resulted in prolonged Ca^{+2} clearance from the cytosol during diastole. A mean decay time of 567.2±16.2 ms was measured after HFpEF induction, compared with a significantly shorter, 505.5±16.9 ms for control (P=0.015; Figure 3C; Table S13). Real-time PCR analysis revealed that SERCA (sarcoplasmic/endoplasmic reticulum Ca^{+2} ATPase) expression did not change significantly in HFpEF-induced cardiomyocytes compared with the control, 1.00±0.17-fold change versus 1.03±0.11 (P=0.90; Figure 3D; Table S14).

Finally, we examined the oxidative stress in the tissues, which is known as a mediator of several pathophysiological mechanisms associated with HFpEF including increased production of ROS, mitochondrial dysfunction, and impaired energetic status. ROS content was significantly elevated in HFpEF conditions: 26 350±1494 arbitrary units (a.u.). in HFpEF tissues versus 19 750±1971 a.u. in control organoids media (P=0.026; Figure 4A; Table S15). Real-time PCR analysis revealed a 12.48±5.7-fold nominal increase in *NOS2* expression without reaching statistical significance (P=0.122; Table S16), encoding iNOS, a key factor in the pathophysiology of oxidative stress in HFpEF. Expression of the *XBP1s* (spliced *XBP1* [Xbox-binding protein 1]), the active form, affecting as a transcription factor of endoplasmic reticulum stress genes, was unchanged 1.39±0.23 (P=0.358; Table S16). The transcription of the inactive form, the XBP1u (unspliced XBP1) was significantly increased by 2.48±0.43-fold (P=0.0375; Figure 4B; Table S16). A study of mitochondrial function revealed a decreased OCR of 256.9±4.4 pmol/min after exposure to HFpEF conditions, compared with 366.7±15.8 pmol/min in the control (P<0.001; Figure 4C; Table S17). ATP content was decreased accordingly, with 413 935±6606 a.u. in HFpEF versus 517 487±8187 a.u. in control using CellTiter-Glo 2.0 ATP assay (P<0.001; Figure 4D; Table S18). Taken together, these findings demonstrate the induction of oxidative stress and metabolic dysfunction after exposure to HFpEF conditions.

DISCUSSION

HFpEF is a rapidly growing global disorder, typically resulting from the interplay of diabetes, hypertension, and obesity, and often serving as a shared end point for these detrimental conditions.[29] Although our comprehension of the pathophysiology and mediators of HFpEF has significantly improved in recent decades, progress in developing remedies for the disease has been limited.[3,30,31] Alongside the recent progress in animal models of HFpEF,[6,32] we anticipate that the introduction of a human, organoid-based model of HFpEF will further enhance the identification of novel therapeutic targets aimed at preventing or mitigating the disease.

In the present study, we generated a novel human in vitro platform that emulates the typical and most common pathological conditions associated with HFpEF. We have shown that exposure of the organoids to a combination of comorbidity-inspired conditions resulted in a synergistic effect ultimately manifesting as cellular and tissue hypertrophy, ultrastructural fibrosis, and abnormal relaxation, the pathophysiological hallmarks of HFpEF. Consequently, we opted to use the combination of the comorbidities-mimicking conditions as the HFpEF inducers. Through comprehensive physiological assessments

Figure 2 Continued. of length increments up to a 0.8 mm stretch. **B** and **C**, Linear regression of the passive force of the hCOs exposed to control (**B**; 6 biological replicates) and HFpEF conditions (**C**; 7 biological replicates), measured as the force (mN) applied after each 0.1 mm preload stretch. **D**, Statistical analysis of maximal passive force (mN) measured after a 0.8 mm stretch. Five and 7 biological replicates were analyzed in the control and HFpEF groups, respectively, using the Mann-Whitney *U* test. **E**, Linear regression of active contraction force (mN) over increasing preload stretches (mm). The number of biological replicates for the control and HFpEF-hCOs was 4 and 6, respectively. The data are presented as linear regression lines and SE bands. **F**, Analysis of NT-proBNP (N-terminal pro-B-type natriuretic peptide) levels (pg/mL) in the media of the exposed organoids. Nine and 7 biological replicates were analyzed in the control and HFpEF groups, respectively, using the Mann-Whitney *U* test. **G**, Immunofluorescence staining of hCOs. Representative images (**left**) and quantification of sarcomeric cTnT (cardiac troponin T) area (μm^2) normalized to nuclei quantity (**right**) are presented. Five and 9 biological replicates were analyzed in the control and HFpEF groups, respectively, using Student *t* test. DAPI indicates 4′,6-diamidino-2-phenylindole. *P<0.05, **P<0.01.

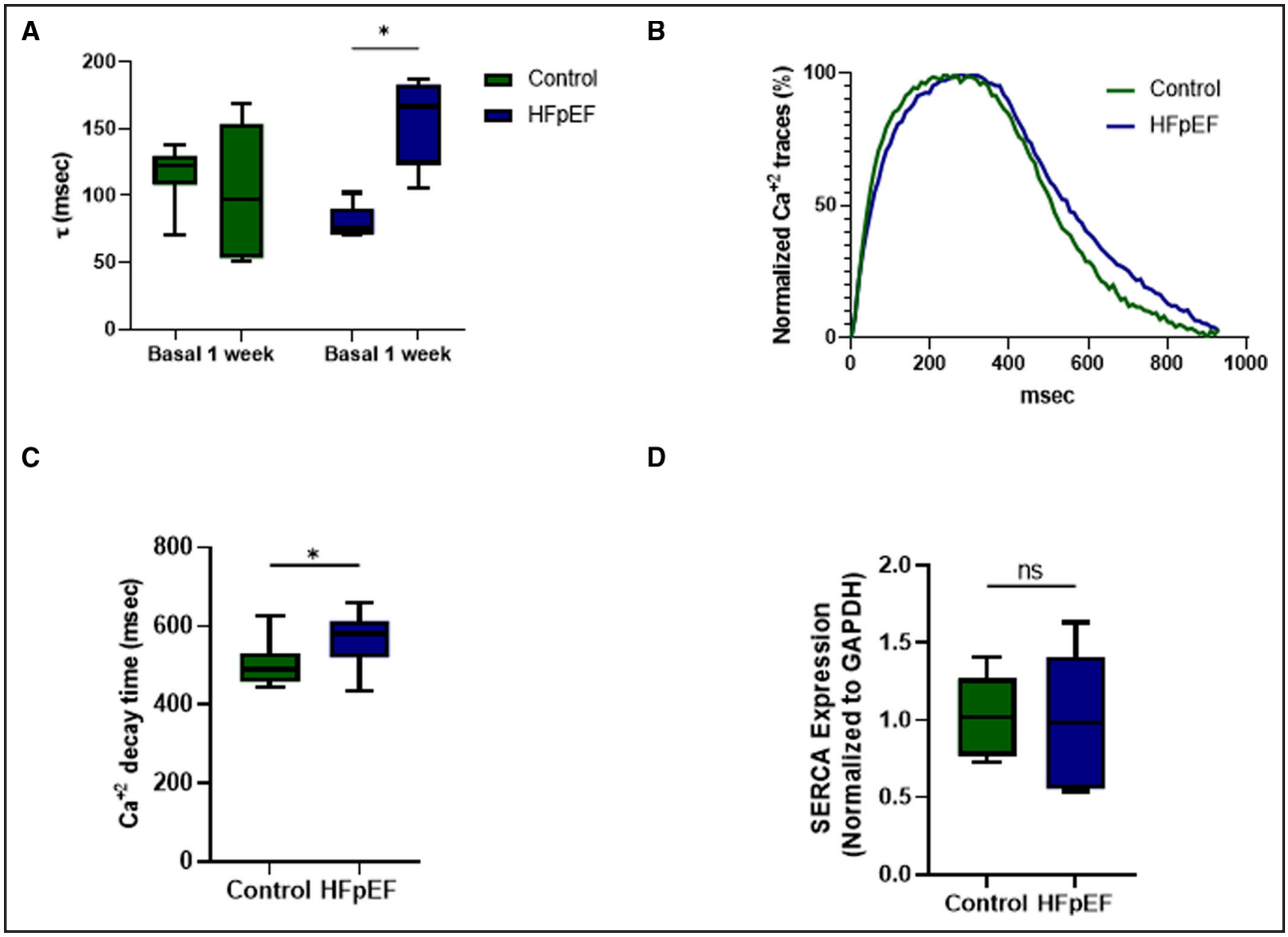

Figure 3. Diastolic evaluation of heart failure with preserved ejection fraction (HFpEF) induction.
A, Relaxation constant τ (tau) of the human cardiac organoids (hCOs) contraction (ms) pre−1 week and post−1 week exposure. Six and 5 biological replicates were analyzed in the control and HFpEF groups, respectively, using repeated-measure 2-way ANOVA. **B**, Representative calcium transients of single contraction cycles, from 0% (baseline) to 100% (peak). **C**, Calcium decay time of the calcium transients (ms). Overall, 12 and 15 biological replicates were analyzed in the control and HFpEF groups, respectively, using Student *t* test. **D**, Real-time polymerase chain reaction of *ATP2A* gene, encoding SERCA (sarcoplasmic/endoplasmic reticulum Ca^{+2} ATPase). Relative expressions were normalized to *GAPDH*. Six biological replicates in each group were analyzed using a Student *t* test. NS indicates nonsignificant. **P*<0.05.

that integrate dynamics of force-length relationships, we have illustrated that subjecting the organoids to the HFpEF-inducing conditions leads to significantly increased passive stiffness, extended relaxation periods, and prolonged calcium decay. Finally, our findings reveal that cardiac organoids exposed to HFpEF-inducing conditions exhibit the key pathophysiological characteristics of the disorder such as increased levels of ROS[33,34] and compromised energetic status as evidenced by reduced OCRs and diminished ATP content.[15,35,36]

Disease models are vital for gaining a profound understanding of the pathophysiology of human illnesses and are nearly always indispensable for identifying novel therapeutic targets and for drug development.[5,19] Recent advancements in the field of in vivo modeling further enhance our understanding of HFpEF and elegantly demonstrate that several hits are required to more thoroughly emulate the disease phenotype.[4,5,11,32] The multihit strategy for the development of HFpEF in vivo models includes perturbations related to senescence and aging,[37] emulation of hypertension,[38] and inducers mimicking cardiometabolic disorders such as high-fat diet and nitrosative stress.[11] The ZSF1 (Zucker fatty spontaneously hypertensive F1 hybrid) rats,[32] derived from crossing Zucker diabetic fatty rats with spontaneously hypertensive heart failure rat strains, are widely recognized as a reliable model for HFpEF.[5] Their development underscores the importance of incorporating various comorbidity-inspired modifications to induce the disease phenotype accurately.[39] One of the key mechanistic insights derived from the in vivo models is that HFpEF is driven by a metabolic inflammation (meta-inflammation) resulting in impaired myocardial energetics.[40–42] Although animal models offer valuable insights, both in general and particularly for HFpEF modeling, they possess inherent limitations stemming from fundamental interspecies differences in cardiovascular physiology (eg, the resting heart is about 5-fold higher in rodents). Finally,

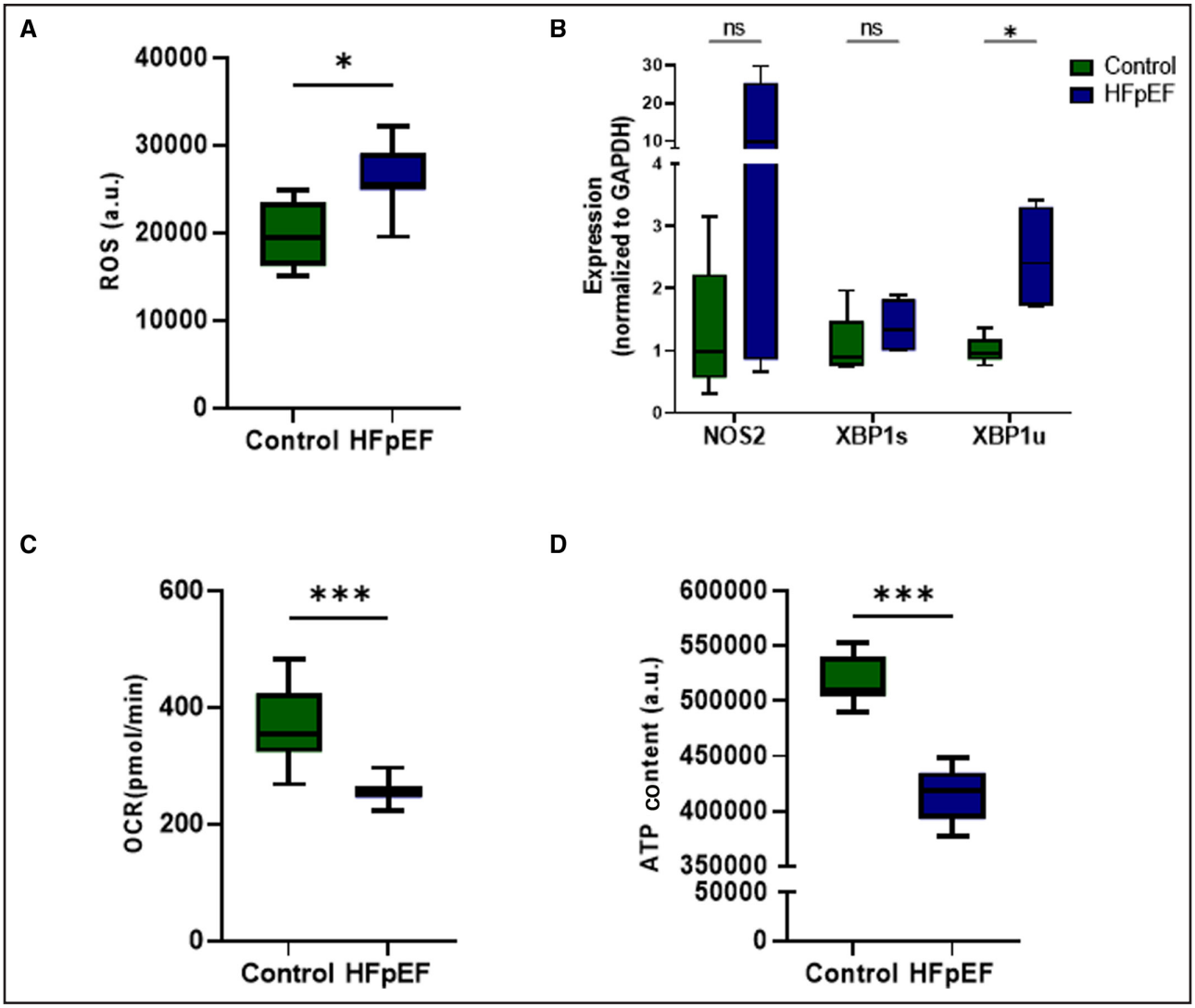

Figure 4. Oxidative stress and energetics evaluation in cardiomyocytes exposed to heart failure with preserved ejection fraction (HFpEF)–mimicking conditions.

A, Reactive oxygen species (ROS) content. Four and 7 biological replicates were analyzed in the control and HFpEF groups, respectively. Measured in arbitray units (a.u.). **B**, Real-time polymerase chain reaction of oxidative stress–related genes: XBP1s (spliced Xbox-binding protein 1), XBP1u (unspliced Xbox-binding protein 1), and *NOS2* (NO synthase 2), encoding *iNOS* (inducible NO synthase). Five to 6 biological replicates were analyzed in the control and HFpEF groups. Relative expressions were normalized to *GAPDH*. **C**, Mitochondrial activity, measured by the basal oxygen consumption rate (OCR), in pmol/min. Sixteen biological replicates were analyzed in both groups. **D**, ATP content, measured by the fluorescence of the ATP indicator. Seven and 12 biological replicates were analyzed in the control and HFpEF groups. Measured in a.u. A Student *t* test was performed in **A** through **D**. **P*<0.05, ***P*<0.01, ****P*<0.001.

cardiovascular animal models have demonstrated limited reproducibility and a weak correlation with data from human clinical trials, both overall[43,44] and specifically in the case of HFpEF.[45,46]

The advent of hiPSC-based heart organoids induced a paradigm shift in the ability to study cardiovascular diseases and cardiac pharmacology.[47] Over the past decade, hiPSC and hiPSC-based cardiovascular organoids have proven to be useful in deciphering the pathophysiology of genetic cardiomyopathies.[23,24,48–50] More recently, encouraging preliminary findings have emerged regarding acquired cardiomyopathies and drug-induced cardiotoxicity.[22,51–54] There is, however, limited data regarding the ability to model multifactorial disorders such as HFpEF using hiPSC-based organoids. Drawnel et al[55] demonstrated the ability to mimic diabetic cardiomyopathy by using high glucose (10 mM), endothelin-1, and cortisol. The exposed cardiomyocytes presented elevated BNP levels, cellular hypertrophy, and abnormal calcium handling. Granéli et al[56] used a more advanced form of stimulation using higher glucose levels, palmitate, free fatty acids, and uric acid, which resulted in higher natriuretic peptide B/A gene (*NPPB/A*) expression and lower maximal OCR. The current study illustrates the ability to simulate the multifaceted origins of HFpEF, beyond diabetes; we induced perturbations linked to

both inflammations associated with obesity and hypertension. Furthermore, the 3-dimensional organoid model recapitulated the functional phenotype of HFpEF by demonstrating the 2 key pathophysiological hallmarks of HFpEF: increased stiffness and abnormal relaxation (expressed both as tau and prolonged calcium decay).

Beyond the pathophysiological phenotype of HFpEF demonstrated in the generated model, we evaluated several pathogenic mechanisms known to participate in mediating the disorder. Oxidative stress is an important mechanism in the induction of HFpEF,[12,33,57,58] affecting among others fibrosis and impaired energetics.[33,59] In our current study, we showcased increased levels of ROS in cardiomyocytes exposed to HFpEF-inducing conditions. Furthermore, this effect was coupled by upregulation of both *iNOS* (inducible NO synthase) and XBP1 expression, both known to be elevated in HFpEF.[13] Additional factors widely recognized for their role in mediating HFpEF include mitochondrial dysfunction and abnormal energetics.[14,15,60] In the current work, we demonstrate a compromised level of both total ATP and OCR in the generated model.

In vitro models offer a valuable alternative to in vivo approaches. The recent Food and Drug Administration Modernization Act 2.0[61,62] strongly encourages the utilization of animal-free alternatives, such as human organoid models. It emphasizes the significance of human organoid models in faithfully replicating human physiology and disease processes, including those related to the cardiovascular system, and underscores their potential in drug development.[62] Despite the advantages of in vitro HFpEF models in investigating potential treatments and pathophysiology, it is crucial to recognize their limitations, in general, and the limitations of this specific work. The current model is suggested as a complementary model to in vivo models because it cannot replicate the intricate multiorgan environment and the absence of immune cells, which play important roles in HFpEF pathophysiology. The present study provides proof-of-concept for modeling an acquired multifactorial disease, such as HFpEF. The model may be further developed in future studies by incorporating a dimension of multicellularity, potentially offering further mechanistic insights into the interplay between cardiomyocytes and noncardiomyocytes in the pathogenesis of the disease. Acknowledging these limitations, given that, to our knowledge, there are no established and replicable examples of in vitro models for HFpEF in the literature, the novel model suggested herein could offer a promising supplement for bridging gaps and throughput issues currently acquainted with in vivo model of the disease.

In summary, we established a novel, human, organoid-based in vitro model for HFpEF utilizing comorbidity-inspired mimicking conditions. The generated model faithfully recapitulated the structural, functional, electrophysiological, and mechanistic features in a consistently replicable manner. The advent of acquired, multifactorial disease models may allow unparalleled insights into the mechanisms underlying human disorders and facilitate the identification of novel therapeutic targets, both in general and specifically for HFpEF.

ARTICLE INFORMATION

Received February 12, 2024; accepted January 6, 2025.

Affiliations

Bruce Rapport Faculty of Medicine, Technion–Israel Institute of Technology, Haifa, Israel (I.R.H., N.K., C.B., O.C.). The Clinical Research Institute at Rambam, Haifa, Israel (I.R.H., A.G., N.K., C.B., H.L.K., O.C.). The Heart Failure Unit, Department of Cardiology, Rambam Health Care Campus, Haifa, Israel (A.G., H.L.K., O.C.).

Acknowledgments

The authors thank the Biomedical Core Facility staff at the Technion–Israel Institute of Technology for their support in conducting the histological analysis. The authors acknowledge Lior Gepstein's laboratory for their support in providing the facilities and equipment needed to conduct the physiological experiments.

Sources of Funding

The study was supported by academic grants from the Israeli Science Foundation, the Israeli Ministry of Health, and the Israeli Ministry of Science.

Disclosures

Dr Caspi has received speaker honoraria from AstraZeneca, Novo Nordisk, and Pfizer and has received consultancy honoraria from Vectorious Medical Technologies. The other authors report no conflicts.

Supplemental Material

Tables S1–S18
Figures S1–S4

REFERENCES

1. Dunlay SM, Roger VL, Redfield MM. Epidemiology of heart failure with preserved ejection fraction. *Nat Rev Cardiol*. 2017;14:591–602. doi: 10.1038/nrcardio.2017.65
2. Adamczak DM, Oduah M-T, Kiebalo T, Nartowicz S, Bęben M, Pochylski M, Ciepłucha A, Gwizdała A, Lesiak M, Straburzyńska-Migaj E. Heart failure with preserved ejection fraction-a concise review. *Curr Cardiol Rep*. 2020;22:82. doi: 10.1007/s11886-020-01349-3
3. McDonagh TA, Metra M, Adamo M, Gardner RS, Baumbach A, Böhm M, Burri H, Butler J, Čelutkienė J, Chioncel O, et al; ESC Scientific Document Group. 2023 focused update of the 2021 ESC guidelines for the diagnosis and treatment of acute and chronic heart failure. *Eur Heart J*. 2023;44:3627–3639. doi: 10.1093/eurheartj/ehad195
4. Horgan S, Watson C, Glezeva N, Baugh J. Murine models of diastolic dysfunction and heart failure with preserved ejection fraction. *J Card Fail*. 2014;20:984–995. doi: 10.1016/j.cardfail.2014.09.001
5. Roh J, Hill JA, Singh A, Valero-Muñoz M, Sam F. Heart failure with preserved ejection fraction: heterogeneous syndrome, diverse preclinical models. *Circ Res*. 2022;130:1906–1925. doi: 10.1161/CIRCRESAHA.122.320257
6. Gao S, Liu X-P, Li T-T, Chen L, Feng Y-P, Wang Y-K, Yin Y-J, Little PJ, Wu X-Q, Xu S-W, et al. Animal models of heart failure with preserved ejection fraction (HFpEF): from metabolic pathobiology to drug discovery. *Acta Pharmacol Sin*. 2024;45:23–35. doi: 10.1038/s41401-023-01152-0
7. Valero-Muñoz M, Backman W, Sam F. Murine models of heart failure with preserved ejection fraction: a "fishing expedition." *JACC Basic Transl Sci*. 2017;2:770–789. doi: 10.1016/j.jacbts.2017.07.013
8. Borlaug BA. The pathophysiology of heart failure with preserved ejection fraction. *Nat Rev Cardiol*. 2014;11:507–515. doi: 10.1038/nrcardio.2014.83
9. Runte KE, Bell SP, Selby DE, Häußler TN, Ashikaga T, LeWinter MM, Palmer BM, Meyer M. Relaxation and the role of calcium in isolated contracting myocardium from patients with hypertensive heart disease and heart failure with preserved ejection fraction. *Circ Heart Fail*. 2017;10:e004311. doi: 10.1161/CIRCHEARTFAILURE.117.004311

10. Adeniran I, MacIver DH, Hancox JC, Zhang H. Abnormal calcium homeostasis in heart failure with preserved ejection fraction is related to both reduced contractile function and incomplete relaxation: an electromechanically detailed biophysical modeling study. *Front Physiol*. 2015;6:78. doi: 10.3389/fphys.2015.00078
11. Schiattarella GG, Altamirano F, Tong D, French KM, Villalobos E, Kim SY, Luo X, Jiang N, May HI, Wang ZV, et al. Nitrosative stress drives heart failure with preserved ejection fraction. *Nature*. 2019;568:351–356. doi: 10.1038/s41586-019-1100-z
12. Zhazykbayeva S, Hassoun R, Herwig M, Budde H, Kovács A, Mannherz HG, El-Battrawy I, Tóth A, Schmidt WE, Mügge A, et al. Oxidative stress and inflammation distinctly drive molecular mechanisms of diastolic dysfunction and remodeling in female and male heart failure with preserved ejection fraction rats. *Front Cardiovasc Med*. 2023;10:1157398. doi: 10.3389/fcvm.2023.1157398
13. Guo F, Lin EA, Liu P, Lin J, Liu C. XBP1U inhibits the XBP1S-mediated upregulation of the iNOS gene expression in mammalian ER stress response. *Cell Signal*. 2010;22:1818–1828. doi: 10.1016/j.cellsig.2010.07.006
14. Lopaschuk GD, Karwi QG, Tian R, Wende AR, Abel ED. Cardiac energy metabolism in heart failure. *Circ Res*. 2021;128:1487–1513. doi: 10.1161/CIRCRESAHA.121.318241
15. Kumar AA, Kelly DP, Chirinos JA. Mitochondrial dysfunction in heart failure with preserved ejection fraction. *Circulation*. 2019;139:1435–1450. doi: 10.1161/CIRCULATIONAHA.118.036259
16. McKeithan WL, Feyen DAM, Bruyneel AAN, Okolotowicz KJ, Ryan DA, Sampson KJ, Potet F, Savchenko A, Gómez-Galeno J, Vu M, et al. Reengineering an antiarrhythmic drug using patient hiPSC cardiomyocytes to improve therapeutic potential and reduce toxicity. *Cell Stem Cell*. 2020;27:813.e6–821.e6. doi: 10.1016/j.stem.2020.08.003
17. Mehta A, Ramachandra CJA, Singh P, Chitre A, Lua CH, Mura M, Crotti L, Wong P, Schwartz PJ, Gnecchi M, et al. Identification of a targeted and testable antiarrhythmic therapy for long-QT syndrome type 2 using a patient-specific cellular model. *Eur Heart J*. 2018;39:1446–1455. doi: 10.1093/eurheartj/ehx394
18. Bezzerides VJ, Caballero A, Wang S, Ai Y, Hylind RJ, Lu F, Heims-Waldron DA, Chambers KD, Zhang D, Abrams DJ, et al. Gene therapy for catecholaminergic polymorphic ventricular tachycardia by inhibition of Ca^{2+}/calmodulin-dependent kinase II. *Circulation*. 2019;140:405–419. doi: 10.1161/CIRCULATIONAHA.118.038514
19. Hnatiuk AP, Briganti F, Staudt DW, Mercola M. Human iPSC modeling of heart disease for drug development. *Cell Chem Biol*. 2021;28:271–282. doi: 10.1016/j.chembiol.2021.02.016
20. Takahashi K, Yamanaka S. Induction of pluripotent stem cells from mouse embryonic and adult fibroblast cultures by defined factors. *Cell*. 2006;126:663–676. doi: 10.1016/j.cell.2006.07.024
21. Karagiannis P, Takahashi K, Saito M, Yoshida Y, Okita K, Watanabe A, Inoue H, Yamashita JK, Todani M, Nakagawa M, et al. Induced pluripotent stem cells and their use in human models of disease and development. *Physiol Rev*. 2019;99:79–114. doi: 10.1152/physrev.00039.2017
22. Seefeldt JM, Libai Y, Berg K, Jespersen NR, Lassen TR, Dalsgaard FF, Ryhammer P, Pedersen M, Ilkjaer LB, Hu MA, et al. Effects of ketone body 3-hydroxybutyrate on cardiac and mitochondrial function during donation after circulatory death heart transplantation. *Sci Rep*. 2024;14:757. doi: 10.1038/s41598-024-51387-y
23. Caspi O, Huber I, Gepstein A, Arbel G, Maizels L, Boulos M, Gepstein L. Modeling of arrhythmogenic right ventricular cardiomyopathy with human induced pluripotent stem cells. *Circ Cardiovasc Genet*. 2013;6:557–568. doi: 10.1161/CIRCGENETICS.113.000188
24. Giacomelli E, Meraviglia V, Campostrini G, Cochrane A, Cao X, van Helden RWJ, Krotenberg Garcia A, Mircea M, Kostidis S, Davis RP, et al. Human-iPSC-derived cardiac stromal cells enhance maturation in 3D cardiac microtissues and reveal non-cardiomyocyte contributions to heart disease. *Cell Stem Cell*. 2020;26:862.e11–879.e11. doi: 10.1016/j.stem.2020.05.004
25. Stirling DR, Swain-Bowden MJ, Lucas AM, Carpenter AE, Cimini BA, Goodman A. CellProfiler 4: improvements in speed, utility and usability. *BMC Bioinf*. 2021;22:433. doi: 10.1186/s12859-021-04344-9
26. Goldfracht I, Efraim Y, Shinnawi R, Kovalev E, Huber I, Gepstein A, Arbel G, Shaheen N, Tiburcy M, Zimmermann WH, et al. Engineered heart tissue models from hiPSC-derived cardiomyocytes and cardiac ECM for disease modeling and drug testing applications. *Acta Biomater*. 2019;92:145–159. doi: 10.1016/j.actbio.2019.05.016
27. Guatimosim S, Guatimosim C, Song L-S. Imaging calcium sparks in cardiac myocytes. *Methods Mol Biol*. 2011;689:205–214. doi: 10.1007/978-1-60761-950-5_12
28. Gu X, Ma Y, Liu Y, Wan Q. Measurement of mitochondrial respiration in adherent cells by seahorse XF96 cell Mito stress test. *STAR Protocols*. 2021;2:100245. doi: 10.1016/j.xpro.2020.100245
29. Borlaug BA, Sharma K, Shah SJ, Ho JE. Heart failure with preserved ejection fraction: JACC scientific statement. *J Am Coll Cardiol*. 2023;81:1810–1834. doi: 10.1016/j.jacc.2023.01.049
30. Anker SD, Butler J, Filippatos G, Ferreira JP, Bocchi E, Böhm M, Brunner-La Rocca H-P, Choi D-J, Chopra V, Chuquiure-Valenzuela E, et al; EMPEROR-Preserved Trial Investigators. Empagliflozin in heart failure with a preserved ejection fraction. *N Engl J Med*. 2021;385:1451–1461. doi: 10.1056/NEJMoa2107038
31. Solomon SD, McMurray JJV, Anand IS, Ge J, Lam CSP, Maggioni AP, Martinez F, Packer M, Pfeffer MA, Pieske B, et al; PARAGON-HF Investigators and Committees. Angiotensin-neprilysin inhibition in heart failure with preserved ejection fraction. *N Engl J Med*. 2019;381:1609–1620. doi: 10.1056/NEJMoa1908655
32. Schauer A, Draskowski R, Jannasch A, Kirchhoff V, Goto K, Männel A, Barthel P, Augstein A, Winzer E, Tugtekin M, et al. ZSF1 rat as animal model for HFpEF: development of reduced diastolic function and skeletal muscle dysfunction. *ESC Heart Fail*. 2020;7:2123–2134. doi: 10.1002/ehf2.12915
33. Faria A, Persaud SJ. Cardiac oxidative stress in diabetes: mechanisms and therapeutic potential. *Pharmacol Ther*. 2017;172:50–62. doi: 10.1016/j.pharmthera.2016.11.013
34. van der Pol A, van Gilst WH, Voors AA, van der Meer P. Treating oxidative stress in heart failure: past, present and future. *Eur J Heart Fail*. 2019;21:425–435. doi: 10.1002/ejhf.1320
35. Schwartz B, Gjini P, Gopal DM, Fetterman JL. Inefficient batteries in heart failure: metabolic bottlenecks disrupting the mitochondrial ecosystem. *JACC Basic Transl Sci*. 2022;7:1161–1179. doi: 10.1016/j.jacbts.2022.03.017
36. Yoshii A, Tian R. Remodeling of cardiac metabolism in heart failure with preserved ejection fraction. *Curr Opin Physiol*. 2022;27:100559. doi: 10.1016/j.cophys.2022.100559
37. Roh JD, Houstis N, Yu A, Chang B, Yeri A, Li H, Hobson R, Lerchenmüller C, Vujic A, Chaudhari V, et al. Exercise training reverses cardiac aging phenotypes associated with heart failure with preserved ejection fraction in male mice. *Aging Cell*. 2020;19:e13159. doi: 10.1111/acel.13159
38. Regan JA, Mauro AG, Carbone S, Marchetti C, Gill R, Mezzaroma E, Valle Raleigh J, Salloum FN, Van Tassell BW, Abbate A, et al. A mouse model of heart failure with preserved ejection fraction due to chronic infusion of a low subpressor dose of angiotensin II. *Am J Physiol Heart Circ Physiol*. 2015;309:H771–H778. doi: 10.1152/ajpheart.00282.2015
39. Deng Y, Xie M, Li Q, Xu X, Ou W, Zhang Y, Xiao H, Yu H, Zheng Y, Liang Y, et al. Targeting mitochondria-inflammation circuit by β-Hydroxybutyrate mitigates HFpEF. *Circ Res*. 2021;128:232–245. doi: 10.1161/CIRCRESAHA.120.317933
40. Schiattarella GG, Altamirano F, Kim SY, Tong D, Ferdous A, Piristine H, Dasgupta S, Wang X, French KM, Villalobos E, et al. Xbp1s-FoxO1 axis governs lipid accumulation and contractile performance in heart failure with preserved ejection fraction. *Nat Commun*. 2021;12:1684. doi: 10.1038/s41467-021-21931-9
41. Tong D, Schiattarella GG, Jiang N, Altamirano F, Szweda PA, Elnwasany A, Lee DI, Yoo H, Kass DA, Szweda LI, et al. NAD+ repletion reverses heart failure with preserved ejection fraction. *Circ Res*. 2021;128:1629–1641. doi: 10.1161/CIRCRESAHA.120.317046
42. Schiattarella GG, Rodolico D, Hill JA. Metabolic inflammation in heart failure with preserved ejection fraction. *Cardiovasc Res*. 2021;117:423–434. doi: 10.1093/cvr/cvaa217
43. Cho S, Discher DE, Leong KW, Vunjak-Novakovic G, Wu JC. Challenges and opportunities for the next generation of cardiovascular tissue engineering. *Nat Methods*. 2022;19:1064–1071. doi: 10.1038/s41592-022-01591-3
44. Savoji H, Mohammadi MH, Rafatian N, Toroghi MK, Wang EY, Zhao Y, Korolj A, Ahadian S, Radisic M. Cardiovascular disease models: a game changing paradigm in drug discovery and screening. *Biomaterials*. 2019;198:3–26. doi: 10.1016/j.biomaterials.2018.09.036
45. Van Tassell BW, Trankle CR, Canada JM, Carbone S, Buckley L, Kadariya D, Del Buono MG, Billingsley H, Wohlford G, Viscusi M, et al. IL-1 blockade in patients with heart failure with preserved ejection fraction. *Circ Heart Fail*. 2018;11:e005036. doi: 10.1161/CIRCHEARTFAILURE.118.005036
46. Toldo S, Mezzaroma E, Bressi E, Marchetti C, Carbone S, Sonnino C, Van Tassell BW, Abbate A. Interleukin-1β blockade improves left ventricular systolic/diastolic function and restores contractility reserve in severe ischemic cardiomyopathy in the mouse. *J Cardiovasc Pharmacol*. 2014;64:1–6. doi: 10.1097/FJC.0000000000000106

47. Kostina A, Volmert B, Aguirre A. Human heart organoids: current applications and future perspectives. *Eur Heart J*. 2023;45:751–753. doi: 10.1093/eurheartj/ehad841
48. Itzhaki I, Maizels L, Huber I, Zwi-Dantsis L, Caspi O, Winterstern A, Feldman O, Gepstein A, Arbel G, Hammerman H, et al. Modelling the long QT syndrome with induced pluripotent stem cells. *Nature*. 2011;471:225–229. doi: 10.1038/nature09747
49. Caspi O, Gepstein L. Insights from the third dimension: cardiac organoids help identify regenerative pathways. *Cell Stem Cell*. 2019;24:833–834. doi: 10.1016/j.stem.2019.05.012
50. Lewis-Israeli YR, Wasserman AH, Gabalski MA, Volmert BD, Ming Y, Ball KA, Yang W, Zou J, Ni G, Pajares N, et al. Self-assembling human heart organoids for the modeling of cardiac development and congenital heart disease. *Nat Commun*. 2021;12:5142. doi: 10.1038/s41467-021-25329-5
51. Mourad O, Yee R, Li M, Nunes SS. Modeling heart diseases on a chip: advantages and future opportunities. *Circ Res*. 2023;132:483–497. doi: 10.1161/CIRCRESAHA.122.321670
52. Gintant G, Burridge P, Gepstein L, Harding S, Herron T, Hong C, Jalife J, Wu JC. Use of human induced pluripotent stem cell-derived cardiomyocytes in preclinical cancer drug cardiotoxicity testing: a scientific statement from the American Heart Association. *Circ Res*. 2019;125:e75–e92. doi: 10.1161/RES.0000000000000291
53. Kitani T, Ong S-G, Lam CK, Rhee J-W, Zhang JZ, Oikonomopoulos A, Ma N, Tian L, Lee J, Telli ML, et al. Human-induced pluripotent stem cell model of trastuzumab-induced cardiac dysfunction in patients with breast cancer. *Circulation*. 2019;139:2451–2465. doi: 10.1161/CIRCULATIONAHA.118.037357
54. Mills RJ, Humphrey SJ, Fortuna PRJ, Lor M, Foster SR, Quaife-Ryan GA, Johnston RL, Dumenil T, Bishop C, Rudraraju R, et al. BET inhibition blocks inflammation-induced cardiac dysfunction and SARS-CoV-2 infection. *Cell*. 2021;184:2167.e22–2182.e22. doi: 10.1016/j.cell.2021.03.026
55. Drawnel FM, Boccardo S, Prummer M, Delobel F, Graff A, Weber M, Gérard R, Badi L, Kam-Thong T, Bu L, et al. Disease modeling and phenotypic drug screening for diabetic cardiomyopathy using human induced pluripotent stem cells. *Cell Rep*. 2014;9:810–821. doi: 10.1016/j.celrep.2014.09.055
56. Granéli C, Hicks R, Brolén G, Synnergren J, Sartipy P. Diabetic cardiomyopathy modelling using induced pluripotent stem cell derived cardiomyocytes: recent advances and emerging models. *Stem Cell Rev and Rep*. 2019;15:13–22. doi: 10.1007/s12015-018-9858-1
57. Hahn VS, Knutsdottir H, Luo X, Bedi K, Margulies KB, Haldar SM, Stolina M, Yin J, Khakoo AY, Vaishnav J, et al. Myocardial gene expression signatures in human heart failure with preserved ejection fraction. *Circulation*. 2021;143:120–134. doi: 10.1161/CIRCULATIONAHA.120.050498
58. Piatek K, Feuerstein A, Zach V, Rozados da Conceicao C, Beblo A, Belyavskiy E, Pieske-Kraigher E, Krannich A, Schwedhelm E, Hinz S, et al. Nitric oxide metabolites: associations with cardiovascular biomarkers and clinical parameters in patients with HFpEF. *ESC Heart Fail*. 2022;9:3961–3972. doi: 10.1002/ehf2.14116
59. Paulus WJ, Zile MR. From systemic inflammation to myocardial fibrosis: the heart failure with preserved ejection fraction paradigm revisited. *Circ Res*. 2021;128:1451–1467. doi: 10.1161/CIRCRESAHA.121.318159
60. Del Campo A, Perez G, Castro PF, Parra V, Verdejo HE. Mitochondrial function, dynamics and quality control in the pathophysiology of HFpEF. *Biochim Biophys Acta Mol Basis Dis*. 2021;1867:166208. doi: 10.1016/j.bbadis.2021.166208
61. Rand SP, et al. Text: S.5002—117th Congress (2021-2022): FDA Modernization Act 2.0 | Congress.gov | Library of Congress. https://www.congress.gov/bill/117th-congress/senate-bill/5002/text
62. Ahmed SM, Shivnaraine RV, Wu JC. FDA Modernization Act 2.0 paves the way to computational biology and clinical trials in a dish. *Circulation*. 2023;148:309–311. doi: 10.1161/CIRCULATIONAHA.123.065585